Computational Modes in Weather and Climate Models

John Thuburn

College of Engineering, Mathematics and Physical Sciences,
University of Exeter, North Park Road, Exeter,
EX4 4QF, United Kingdom
j.thuburn@exeter.ac.uk

ABSTRACT

This article discusses some of the ways in which linear wave propagation can be misrepresented by numerical methods. Examples include modes that fail to propagate, modes that have group velocity of the wrong sign, the appearance of extra branches in the dispersion relation, and the trapping of waves due to grid inhomogeneities. Some of the consequences for modelling the weather and climate are discussed, including a poor representation of adjustment towards balance, an incorrect response to forcing, and the spurious release of instability. Badly behaved numerical wave solutions are often called *computational modes*. However, in many cases the distinction between computational modes and physical modes is not clear cut, nor is it clear that all types of computational modes are necessarily damaging to the model solution; each case must be examined on its own merits.

1 Introduction

The governing equations of atmospheric dynamics, linearized about a suitable basic state, support a variety of fast (acoustic and inertio-gravity) and slow (Rossby) waves. We might hope that the numerical methods we use in weather and climate models are able to capture the behaviour of these linear waves, as a pre-requisite for accurately solving the fully nonlinear governing equations. However, numerical methods can sometimes support waves that have no counterpart in the physical system, or whose behaviour, e.g. in terms of frequency or structure, is so badly distorted that the physical counterpart is difficult to identify. Such waves are often called *computational modes*, whilst those with an identifiable physical counterpart are called *physical modes*.

There is no widely accepted definition of a computational mode. The most well known examples are waves that fail to propagate, but there are many other kinds of distorted behaviour. Indeed, there are examples in which it may be difficult to decide whether a particular mode is physical or computational, or in which a branch of modes switches behaviour between physical and computational as some parameter is varied, thus blurring the distinction. This article takes a rather broad view of the concept of a computational mode, and surveys some of the ways in which numerical wave propagation can depart from physical wave propagation.

Computational modes can be damaging to weather or climate model solutions in a variety of ways. They may manifest themselves as a noisy solution, a failure to adjust correctly towards balance, a spurious release of instability, or an incorrect response to forcing; some specific examples are given below. In certain numerical calculations computational modes can inhibit convergence. Even if computational modes have zero amplitude in the initial conditions, they will certainly be excited by the nonlinear dynamics, physical parameterizations, boundary conditions, and data assimilation. Computational modes are often characterized by small spatial or temporal scales. This means it may be feasible to suppress them using a suitable scale-selective filter, but such tactics effectively coarsen the resolution of the model and are also undesirable.

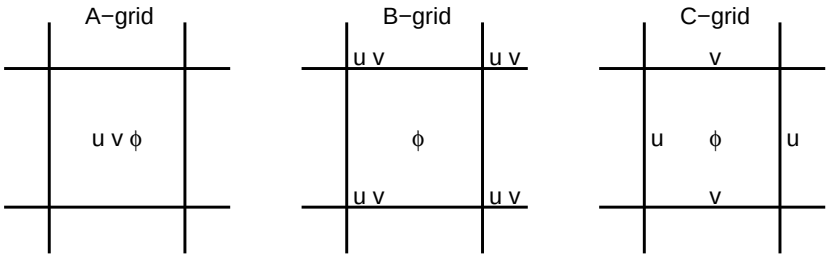

Figure 1: Arrangement of variables on the square A-grid, B-grid and C-grid.

For the sake of clarity, in this article the focus is on simple model problems for which the analysis is relatively tractable and the interpretation relatively straightforward. In practical examples with a more complete model the effects of computational modes can be intermittent, difficult to diagnose, and difficult to disentangle from a host of other complex processes.

2 Classical examples: modes that fail to propagate

This section summarizes some of the most well-known examples of computational modes. They are all examples of non-zero disturbance patterns that are 'invisible' to the dynamics, essentially because of some averaging that hides the small scale structure in one or more variables. A useful technique for analysing the number and type of stationary modes that a given numerical method supports is to examine the kernels of the various linear operators, such as gradient, divergence and Coriolis, that appear (Le Roux et al. 2005, Rostand et al. 2008, Le Roux 2012). Such kernel analysis is complementary to the von Neumann analysis technique discussed below in that it only gives information on stationary modes but is not restricted to grids with discrete translational symmetry.

2.1 Pressure modes

Consider the shallow water equations in Cartesian geometry, linearized about a resting basic state with constant mean geopotential Φ and constant Coriolis parameter f:

$$\phi_t + \Phi(u_x + v_y) = 0, \tag{1}$$
$$u_t - fv + \phi_x = 0, \tag{2}$$
$$v_t + fu + \phi_y = 0. \tag{3}$$

Here, ϕ is the perturbation geopotential and u and v are the perturbation velocity components.

Now consider a centred difference spatial discretization of these equations on a square unstaggered grid. (This arrangement of variables is known as the 'A-grid': Fig. 1.) The discrete velocity equations are

$$\frac{\partial}{\partial t}u_{i,j} - fv_{i,j} + \frac{\phi_{i+1,j} - \phi_{i-1,j}}{2\Delta x} = 0, \tag{4}$$
$$\frac{\partial}{\partial t}v_{i,j} + fu_{i,j} + \frac{\phi_{i,j+1} - \phi_{i,j-1}}{2\Delta y} = 0. \tag{5}$$

Here, i and j are the grid cell indices in the x- and y-directions, respectively, and Δx and Δy are the corresponding grid intervals. It is then clear that an initial condition comprising zero velocity and a checkerboard pattern in ϕ will be steady and so fail to propagate; the finite difference formula estimates the gradient of ϕ as zero.

Similar problems occur with a B-grid (Fig. 1), and with some finite element methods and spectral methods. Such pressure modes are well known throughout computational fluid dynamics and are widely discussed in the literature.

2.2 Velocity modes

Again consider the shallow water equations (1)-(3) discretized on an A-grid. This time restrict attention to the non-rotating case $f = 0$, and consider the discrete mass equation:

$$\frac{\partial}{\partial t}\phi_{i,j} + \Phi\left(\frac{u_{i+1,j} - u_{i-1,j}}{2\Delta x} + \frac{v_{i,j+1} - v_{i,j-1}}{2\Delta y}\right) = 0. \tag{6}$$

An initial condition comprising zero geopotential perturbation and a u field with a $2\Delta x$ wavelength in the x-direction and a v field with a $2\Delta y$ wavelength in the y-direction will be steady and so fail to propagate. In this case the velocity divergence is estimated as zero.

Again similar problems can occur with the B-grid and with certain finite element methods.

2.3 The C-grid Coriolis mode

The fact that it avoids the A-grid and B-grid pressure and velocity modes is one of the reasons for the popularity of the C-grid (Fig. 1) in weather and climate models. On the C-grid the derivatives in (1)-(3) are estimated over a single grid interval, so that the geopotential gradient and velocity divergence are visible even for grid-scale perturbations. The price to pay is that now u and v points are staggered relative to each other, so the Coriolis terms must be averaged:

$$(fv)_{i+1/2,j} \approx \frac{f}{4}\left(v_{i,j-1/2} + v_{i,j+1/2} + v_{i+1,j-1/2} + v_{i+1,j+1/2}\right), \tag{7}$$

$$(fu)_{i,j+1/2} \approx \frac{f}{4}\left(u_{i-1/2,j} + u_{i+1/2,j} + u_{i-1/2,j+1} + u_{i+1/2,j+1}\right). \tag{8}$$

An initial condition with zero ϕ and a non-divergent velocity field with a two-grid-length oscillation in u and v would fail to propagate (Walters and Carey 1984).

Von Neumann analysis (section 3) shows that such Coriolis modes are, in fact, discrete analogues of short wavelength steady geostrophic modes. As such, their zero frequency is actually physically correct behaviour. What is unphysical is their structure; the spurious vanishing of the Coriolis terms due to averaging means that zero amplitude geopotential perturbation is needed to obtain geostrophic balance.

2.4 The Lorenz grid computational mode

Computational modes can also exist associated with the vertical discretization. A well known example occurs with the vertical staggering known as the Lorenz grid (Fig. 2), where we are now considering the fully compressible Euler equations with pressure p and potential temperature θ as prognostic variables. In order to evaluate the vertical pressure gradient term at w-levels, θ must be vertically averaged:

$$c_p\theta \left.\frac{\partial \Pi}{\partial z}\right|_{m+1/2} \approx c_p \overline{\theta}_{m+1/2} \frac{\Pi_{m+1} - \Pi_m}{\Delta z}, \quad \text{where} \quad \overline{\theta}_{m+1/2} = \frac{1}{2}(\theta_m + \theta_{m+1}). \tag{9}$$

(Here m is the vertical level index, being integer at p-levels, $\Pi = (p/p_0)^\kappa$ is the Exner pressure, where p_0 is a constant reference pressure and κ is equal to the gas constant R divided by the specific heat capacity at constant pressure c_p.) Thus, a vertical two-grid-length oscillation can be added to the θ field of any

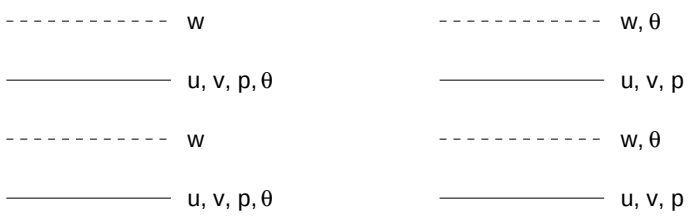

Figure 2: Vertical arrangement of variables on the Lorenz grid (left) and the Charney-Phillips grid (right). Variants with other combinations of prognostic variables exist.

hydrostatically balanced solution to give another hydrostatically balanced solution: the oscillation in θ is invisible to the dynamics.

Essentially the same phenomenon occurs with other forms of vertical averaging (e.g. weighted or geometric mean), with other choices of prognostic thermodynamic variables, and with other forms of the pressure gradient term such as $(1/\rho)\partial p/\partial z$; the computational mode continues to exist, though its structure may be modified. The computational mode also occurs in hydrostatic models; indeed it was first noticed there (Hollingsworth 1995, Tokioka 1978).

When a linear system is forced at the frequency of one of its normal modes, there will usually be a resonant response, with amplitude growing linearly in time. The existence of the computational mode means that a Lorenz grid numerical model will have a spurious resonant response to a steady thermodynamic forcing (Hollingsworth 1995, Schneider 1987). The Lorenz grid computational mode has also been implicated in the spurious release of baroclinic instability (Arakawa and Moorthi 1988).

The Lorenz grid computational mode can be avoided by staggering θ relative to p (or ρ) to obtain the Charney-Phillips grid (Fig. 2), and expressing the pressure gradient term as $c_p\theta\partial\Pi/\partial z$. (Other configurations are also possible, but some care is needed to ensure that the buoyancy term is accurately captured; Thuburn and Woollings 2005, Thuburn 2006, Toy and Randall 2007).

3 Parasitic modes

Each of the examples presented in section 2 is the finest resolvable mode at the end of a spectrum of which a significant part is badly behaved. One of the simplest examples is obtained by considering the one-dimensional, linearized, non-rotating shallow water equations:

$$\phi_t + \Phi u_x = 0, \tag{10}$$

$$u_t + \phi_x = 0. \tag{11}$$

By seeking wavelike solutions proportional to $\exp\{\mathrm{i}(kx-\omega t)\}$, we obtain the dispersion relation

$$\omega^2 = k^2\Phi. \tag{12}$$

The analogous procedure for the discrete case is called *von Neumann Analysis* (e.g. Durran 2010). We seek solutions proportional to $\exp\{\mathrm{i}(ki\Delta x-\omega t)\}$ for a spatial discretization, or to $A^n\exp\{\mathrm{i}(ki\Delta x)\}$ for a space-time discretization, where n is the time step index. The numerical frequency can be inferred from

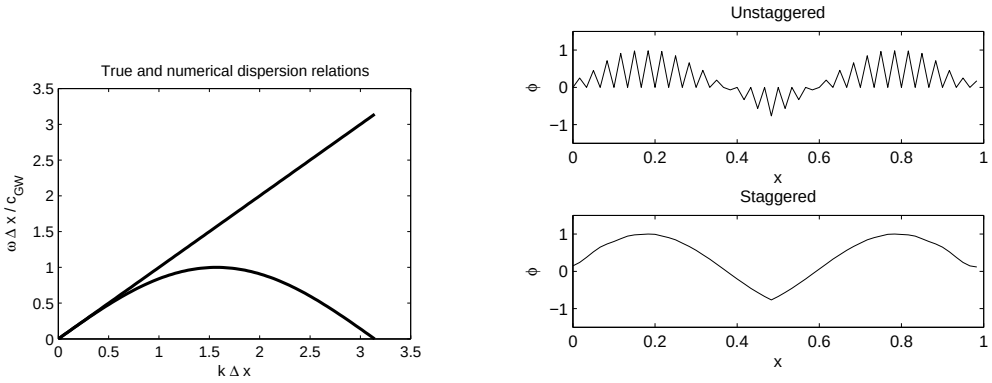

Figure 3: Left: exact and numerical (A-grid) dispersion relations for the one-dimensional non-rotating shallow water equations. Right: response to a slowly oscillating forcing at the centre of the domain; top: on an unstaggered grid (A-grid) a spurious short wavelength response is superposed on the longwave response; bottom: a staggered grid (C-grid) accurately captures the correct longwave response.

the *amplification factor A*. The procedure gives information on the dispersion relation of the discrete system, including its stability.

Figure 3 shows the dispersion relation for the continuous system (12) and for a spatial centred difference discretization on an unstaggered grid (the one-dimensional analogue of the A-grid). Only the positive frequencies are shown. For the shortest resolvable waves, $k\Delta x = \pi$, the numerical frequency is zero; these are the one-dimensional analogues of the pressure and velocity modes of section 2. However, a large part of the numerical spectrum has significantly reduced frequency. In particular, half of the numerical spectrum has $\partial\omega/\partial k$ of the wrong sign implying that packets of such waves have group velocity of the wrong sign. Such modes are often called *parasitic modes* (Trefethen 1982).

The real atmosphere is continually perturbed away from hydrostatic and geostrophic balance by a variety of processes, and adjusts back towards balance through the radiation and eventual dissipation of fast acoustic and inertio-gravity waves. Group velocity errors like those in Fig. 3 severely compromise the ability of a numerical model to capture the adjustment process (Arakawa and Lamb 1977, Randall 1994).

Another undesirable effect arises from the fact that the numerical dispersion relation in Fig. 3 has two values of k for each value of ω. This means that, when forced at a particular frequency, a model can produce a spurious shortwave response as well as a physically realistic longwave response (Fig. 3 right panel).

4 Temporal computational modes, and space-time interaction

Computational modes can be associated with the time discretization as well as the space discretization. They typically occur for schemes that use more than two time levels, such as leapfrog and Adams-Bashforth (e.g. Durran 2010).

Consider a system with N independent prognostic fields. The continuous dispersion relation will be a degree N polynomial in ω, giving N normal modes for each wavenumber. For a two-time-level time discretization, carrying out von Neumann analysis and cancelling excess powers of A leads to N equations, each a polynomial of degree 1 in A. Elimination of unknowns reduces this to a single polynomial of degree N in A, giving N numerical modes for each wavenumber, in agreement with the continuous case. If, instead, we use an M-time-level scheme then each prognostic equation reduces to a polyno-

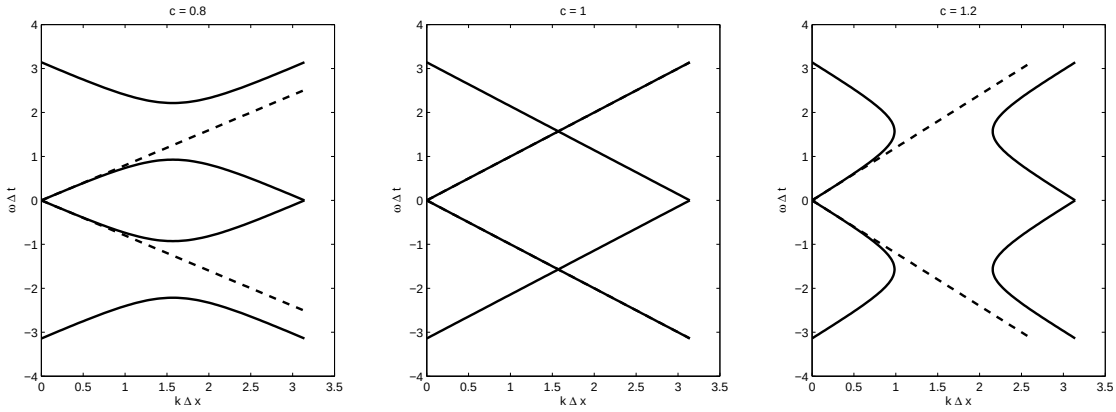

Figure 4: Numerical (solid) and exact (dashed) dispersion relations for the centred-time, centred-space discretization of (10),(11)*. Left:* $c = 0.8$*; centre:* $c = 1$*; right:* $c = 1.2$.

mial of degree $M-1$ in A, which, after elimination of unknowns, boils down to a polynomial of degree $N(M-1)$ in A for the discrete dispersion relation. Thus, for each wavenumber, we obtain an extra $N(M-2)$ modes. In other words, we obtain an extra N *families* of modes for every extra time level.

In the limit of small timestep, $\Delta t \to 0$, a physical mode should change by a vanishingly small amount over one time step, i.e. $A \to 1$. Any mode for which A does not tend to 1 as $\Delta t \to 0$ must therefore be a temporal computational mode.

The leapfrog scheme computational mode is undamped ($|A| = 1$) for an oscillatory system (with small enough Δt) and unstable ($|A| > 1$) for a damped system. Therefore, it must be controlled by some form of temporal filter (Robert 1966, Asselin 1972, Williams 2009). For some schemes, such as the three-step Adams-Bashforth scheme, the computational modes may be inherently strongly damped for small Δt, but care is required because they may become unstable for moderate Δt (e.g. Durran 2010).

The use of a centred in time, centred in space scheme to solve (10), (11) provides a simple but instructive example of the interaction between spatial and temporal computational modes. The continuous system has two prognostic variables and supports two physical modes, i.e. the left and right propagating waves corresponding to the positive and negative roots for ω, for each wavenumber k. Because the numerical scheme involves three time levels we expect to find four values of A, and hence two physical and two computational modes, for each k; this is borne out by von Neumann analysis, which leads to the numerical dispersion relation

$$\sin^2(\omega_{\text{num}}\Delta t) = c^2 \sin^2(k\Delta x), \tag{13}$$

where $c = \Phi^{1/2}\Delta t/\Delta x$ is the wave Courant number, and ω_{num} is the frequency of the numerical solution, which can be deduced from A: $\omega_{\text{num}} = (\mathrm{i}/\Delta t)\ln A$.

This dispersion relation is plotted in Fig. 4 (left panel) for $c = 0.8$, and shows the expected four branches. For the present discussion let us define the physical branches to be those that approach the true dispersion relation as $k\Delta x \to 0$. Then the smaller (positive and negative) frequency branches are the physical modes while the larger (positive and negative) frequency branches are the computational modes. The physical mode branches include the parasitic modes discussed in section 3.

Figure 4 shows what happens to this dispersion relation as c increases to 1 and then 1.2. The physical and computational mode branches merge and then divide again. For $c > 1$ the physical mode branches now have small wavenumbers and the computational mode branches have large wavenumbers; there is an intermediate range of unstable wavenumbers for which there is no real root for ω_{num}. Some modes,

including those that were parasitic modes for $c < 1$, have switched between physical and computational branches.

Although this is a simple example, and the $c > 1$ case is of little practical interest because it is unstable, it makes an important point that the distinction between physical and computational modes might not always be clear cut.

5 Families of spatial computational modes

We have already seen that the use of more than two time levels in the time integration scheme can give rise to entire families of computational modes. Families of computational modes can also arise through the spatial discretization. This is particularly so when we depart from traditional Cartesian or tensor product grids such as latitude-longitude and consider instead grids using different kinds of polygonal cells. Such grids are of increasing interest for ocean modelling, because of the flexibility of polygons in fitting complex coastlines, and for global atmospheric modelling, because they can avoid the polar resolution clustering of the latitude-longitude grid (e.g. Staniforth and Thuburn 2012).

We use the linear, f-plane shallow water equations (1)-(3) for illustration because numerical wave propagation has been relatively well studied for this system. Seeking wavelike solutions of (1)-(3) leads to the continuous dispersion relation

$$\omega(\omega^2 - f^2 - \Phi\mathbf{k}\cdot\mathbf{k}) = 0. \tag{14}$$

For each wavenumber $\mathbf{k} = (k,l)$ there are three roots. The $\omega = 0$ root corresponds to steady geostrophic modes while the other two correspond to eastward and westward propagating inertio-gravity modes.

Provided the grid is sufficiently regular, i.e. provided it has discrete translational symmetry, von Neumann analysis can still be carried out on polygonal grids. The first step is to identify the basic repeating unit of the grid and its associated degrees of freedom. Suppose there are D degrees of freedom per basic repeating unit. The translational symmetry then ensures that wavelike solutions exists for which each of the D degrees of freedom is proportional to $\exp\{\mathrm{i}(\mathbf{k}\cdot\mathbf{x} - \omega t)\}$. Elimination of unknowns then leads to a polynomial of degree D for the frequency ω, implying a numerical dispersion relation with D branches. If $D > 3$ then the excess branches might correspond to families of computational modes.

Such von Neumann analysis has been used on polygonal analogues of the A-, B-, and C-grids, as well as on a variety of finite element schemes (e.g. Le Roux et al. 2007, Le Roux 2012; again D degrees of freedom per basic repeating unit leads to a dispersion relation with D branches). Polygonal A-grids suffer from parasitic modes like those discussed section 3 (e.g. Ničković et al. 2002), so much recent interest has focused on polygonal C-grids. The triangular and hexagonal C-grids are discussed in the following subsections.

5.1 Triangular C-grid

Polygonal C-grids generalize the square C-grid of Fig. 1 by storing ϕ at cell centres and normal velocity components at cell edges. Figure 5 shows the basic repeating unit on the triangular C-grid. There are two ϕ degrees of freedom, one in each triangle, and three velocity degrees of freedom. (The velocity degrees of freedom at the other two edges belong to adjacent repeating units.)

As expected, von Neumann analysis leads to a quintic dispersion relation (Danilov 2010):

$$\frac{\omega}{f}\left\{\left(\frac{\omega}{f}\right)^4 - \left(\frac{\omega}{f}\right)^2 (3Q+C) + 3Q^2(1-C) + Q(4C-1)\right\} = 0, \tag{15}$$

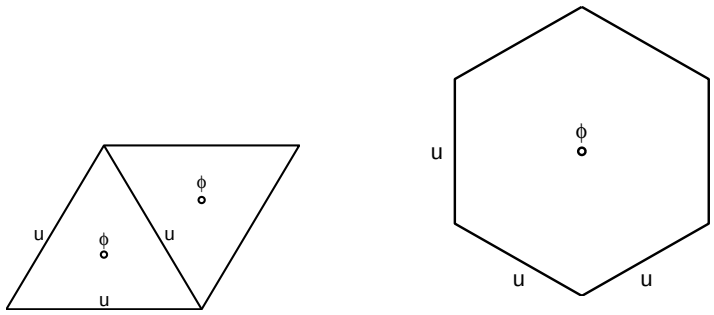

Figure 5: Basic repeating unit on the triangular C-grid (left) and hexagonal C-grid (right), showing the locations of the geopotential and normal velocity degrees of freedom.

where $Q = 8\alpha^2/3$, $\alpha = \Phi^{1/2}/fd$ is the Rossby radius divided by d the distance between adjacent triangle centroids, and C is a function of the wavenumber $\mathbf{k}$.

The $\omega = 0$ root corresponds to steady geostrophic modes, two of the non-zero roots correspond to inertio-gravity modes, and the other two correspond to inertio-gravity-like modes. (A rule of thumb for C-grids is that the number of geostrophic mode branches is given by the number of vorticity degrees of freedom, i.e. the number of grid vertices, per basic repeating unit, while the number of inertio-gravity mode branches is given by the number of mass plus divergence degrees of freedom, i.e. twice the number of cells, per basic repeating unit.)

It is tempting to interpret the fourth and fifth roots as computational modes. However, the issue is complicated by the fact that there are enough degrees of freedom per basic repeating unit to support some internal structure. Hence, a mode corresponding to a particular value of $\mathbf{k}$ in the von Neumann analysis might represent a mode of a larger wavenumber that is aliased into $\mathbf{k}$. The possibility that the fourth and fifth branches might actually represent physically reasonable extensions to higher wavenumber of the second and third branches must be carefully checked by examining the mode structures and frequencies.

Figure 6 shows the two positive frequency branches for various values of α. For small values of k, ω/f should approach 1, which it always does for one of the branches. Thus, this branch must be the unaliased one for which the mode wavenumber agrees, at least approximately, with the von Neumann analysis k. For large values of α, the two branches appear to cross at wavenumber $k_{\text{cross}}\Delta x \approx 2.42$, suggesting that the upper branch might be a physically reasonable branch whose true wavenumber $2k_{\text{cross}} - k$ is aliased into k. However, there are two flaws with this suggestion. First, k_{cross} is different from the maximum resolvable wavenumber $k_{\max}d = 2\pi/\sqrt{3}$, so some some wavenumbers would still be duplicated. Second, the branches approach each other but do not actually cross; there is a small frequency gap. For smaller α the gap is more noticeable. Thus although the aliased branch in some ways resembles a plausible extension of the physical (unaliased) mode branch, in other ways it is unphysical.

For large α the aliased branch sits above the unaliased branch while for small values of α it sits below. For $\alpha = 1/(2\sqrt{2})$ the two branches touch at $k = 0$ and exchange roles. This is another example in which the distinction between physical and computational modes is blurred.

An almost identical phenomenon occurs with the RT0-P0 finite element pair on triangular grids (Le Roux et al. 2007). This should not be too surprising, since the placement of geopotential and velocity degrees of freedom is the same as on the triangular C-grid.

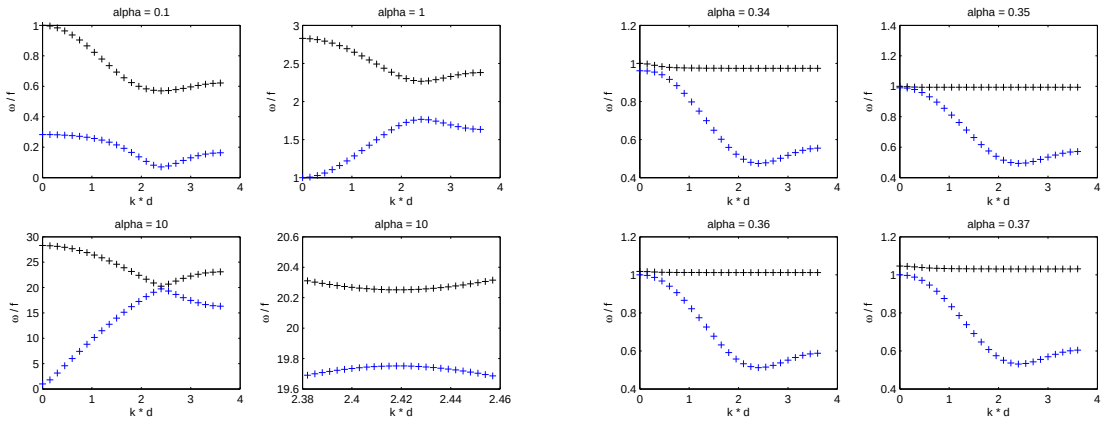

Figure 6: Positive frequency branches of the triangular C-grid dispersion relation (15) *(ω/f vs $k\Delta x$ with $l = 0$) for various values of α.*

5.2 Hexagonal C-grid

Figure 5 shows the basic repeating unit on the hexagonal C-grid. It has one ϕ degree of freedom and three velocity degrees of freedom. Thus we expect a quartic numerical dispersion relation, and this is confirmed by von Neumann analysis (Thuburn 2008):

$$\left(\frac{\omega}{f}\right)^2 \left\{ \left(\frac{\omega}{f}\right)^2 - [T(\mathbf{k}) + QS(\mathbf{k})] \right\} = 0, \tag{16}$$

where T and S are functions of $\mathbf{k}$. There are two branches of zero frequency geostrophic modes and two branches of inertio-gravity modes. (Note that special care is needed in the discretization of the Coriolis terms, otherwise there are no steady modes, Ničković et al. 2002, Thuburn 2008.)

The extra branch is now a branch of geostrophic modes. Again a careful examination is needed to determine whether or not it can be interpreted as a physically reasonable aliased extension of the unaliased physical branch. For the f-plane case that leads to (16) all the geostrophic mode frequencies are exactly zero, which is physically correct. Moreover, the mode structures on the second geostrophic branch are indeed plausible approximations to higher wavenumber modes. Thus, on the basis of this f-plane analysis, we might be justified in interpreting the second geostrophic mode branch as an aliased extension of the physical geostrophic mode branch.

It is only when we introduce a β effect, providing a Rossby wave propagation mechanism, that unphysical behaviour becomes apparent. (We must then make a quasigeostrophic approximation to make the von Neumann analysis tractable, Thuburn 2008.) The second branch modes are then found to have positive frequency (for positive k), whereas we might expect negative frequency for Rossby modes (Fig. 7). This would, in fact, be acceptable if we could interpret the true wavenumber of the modes as having a negative zonal component (aliasing into the positive k of the von Neumann analysis). However, the magnitude of the mode frequency is also much smaller than that of the continous equation mode it is supposed to approximate. Moreover, the mode frequencies on the second Rossby mode branch are very strongly sensistive to the details of the discretization of the Coriolis term, whereas the frequencies of the other three branches are much more robust.

Thus, there are some unphysical aspects of the second Rossby mode branch that could justify calling it a computational mode branch, though these are rather more subtle than in the case of the triangular C-grid. As on the triangular C-grid, there can be an exchange of roles between physical and computational

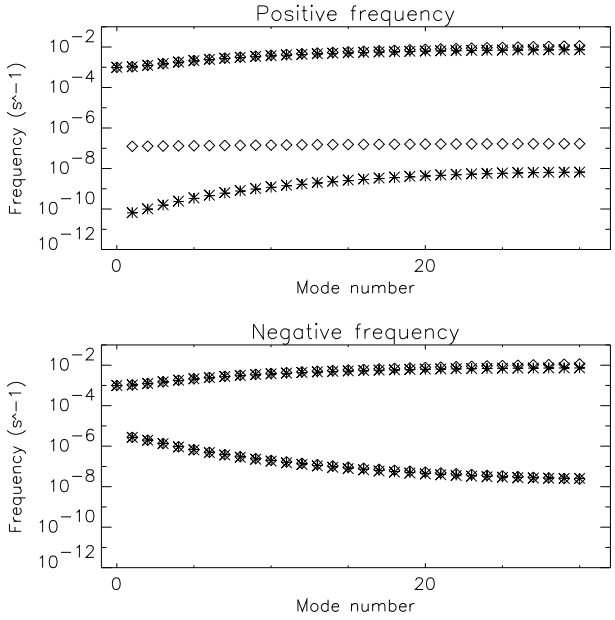

Figure 7: Four branches of the β-plane dispersion relation for the hexagonal C-grid. Crosses are theoretical predictions. Plus symbols are from a numerical eigenvalue calculation in a channel. Diamonds are for the continuous equations. Frequencies greater than $10^{-1}\,\mathrm{s}^{-1}$ in magnitude are for inertio-gravity modes. Smaller negative frequencies are for the physical Rossby mode branch. Smaller positive frequencies are for the second Rossby mode branch (crosses and pluses) or for modes that would alias into the plotted mode number at this resolution (diamonds).

branches as parameters are varied (e.g. Fig. 6 of Thuburn 2008).

The main inaccuracy of the second Rossby mode branch is that the frequencies are too small. However, small scale Rossby modes do have very small intrinsic frequency anyway, so that, in the presence of a background flow (which is usually omitted in the von Neumann analysis), the associated potential vorticity field is advected almost passively by the background flow. The fact that the second branch Rossby modes are excessively passive then makes negligible difference to the behaviour. This argument suggests that the extra Rossby mode branch might be relatively harmless in practice, if not positively beneficial (by providing extra resolution for potential vorticity). Experience with the MPAS hexagonal C-grid atmosphere and ocean models (W. Skamarock, T. Ringler, personal communication) and with a hexagonal C-grid shallow water model developed under the Gung-Ho project has not revealed any problems that can be attributed to the second Rossby mode branch. Focused efforts to devise an idealized test problem that would reveal a damaging effect of the second Rossby mode branch have not yet revealed any such problem (A. Staniforth, personal communication).

6 Trapped modes

Most of our understanding of numerical wave disperson comes from regular grid cases for which progress can be made through mathematical analysis. On irregular grids, such as stretched grids, the behaviour can be significantly more complex. One interesting phenomenon is that waves can be refracted, reflected, or even trapped by grid inhomogeneities.

For the simplest problems on one-dimensional grids some analytical progress is still possible (e.g. Vichnevetsky 1987, Long and Thuburn 2011). For conservative centred difference methods it can be shown that a wave packet will be reflected from a location on the grid where its numerical group velocity

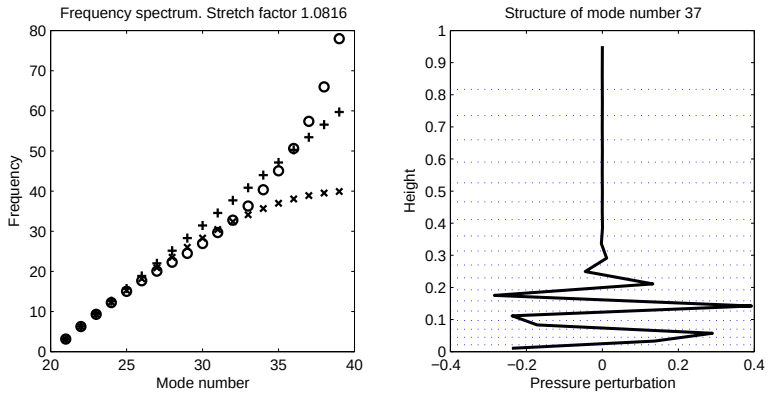

Figure 8: Left: normal mode frequencies (only positive frequencies shown) for the system (17)*: continuous equations (+ symbols), uniform grid (x symbols), and stretched grid with successive layer thicknesses in the ratio* 1.04^2 *(circles). Right: p-structure of the* 37^{th} *stretched grid normal mode showing trapping in the fine-resolution part of the grid.*

goes to zero; the reflected wave may have the same wavelength as the incident wave packet, or may be converted into a parasitic mode, depending on the details of the numerical method.

The possibility of trapping has consequences for the spectrum of normal modes on non-uniform grids. (In these more complex problems mathematical analysis becomes intractable; to make progress the system matrix must be built and its eigenvalues found numerically.) Figure 8 shows the frequency spectrum for the simple acoustic wave system

$$p_t + c^2 w_z = 0, \qquad w_t + p_z = 0, \tag{17}$$

solved numerically on a stretched grid of 20 levels. At first glance the higher frequencies appear to be closer to the continuous dispersion relation than the numerical frequencies for a uniform grid. However, examination of the mode structures for the higher frequency modes shows that they are in fact trapped in the finer resolution region of the grid.

Another example, taken from Weller et al. (2012), is shown in Fig. 9. It shows the highest frequency eigenmode for the linearized shallow water equations on a rotating sphere found numerically on coarse versions of three different spherical C-grids. On each grid, the mode is trapped in regions of the grid that have finer grid cells than elsewhere, giving a two-dimensional analogue of the one-dimensional trapping shown in Fig. 8.

7 Conclusions

Linear wave propagation can be misrepresented by numerical methods in a variety of ways. Examples presented here include modes that fail to propagate, parasitic modes with reversed group velocity, the appearance of extra branches of modes in the dispersion relation due to either the time or space discretization, and wave trapping by grid inhomogeneities. Such poor wave behaviour can be damaging to weather and climate model numerical solutions, for example leading to a noisy solution, a failure to adjust correctly towards balance, a spurious release of instability, or an incorrect response to forcing.

The degree to which a given mode or branch of modes misrepresents the physics, and therefore damages the solution, can vary considerably. It is therefore not straightforward to give a universally applicable definition of *computational mode*. Indeed, modes can switch between physical-mode-like and

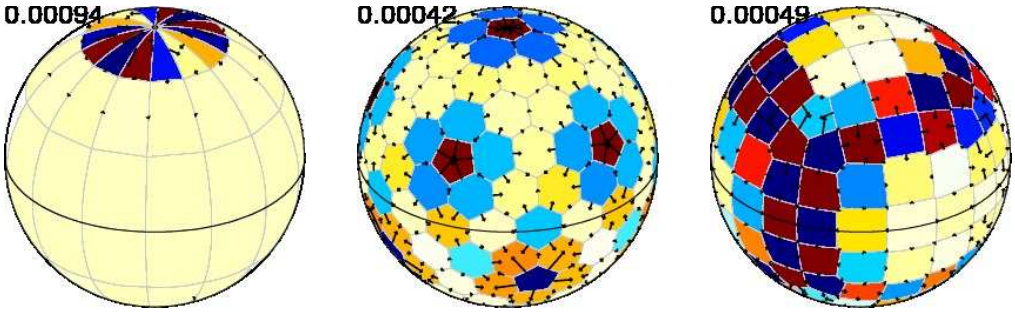

Figure 9: Geopotential structure of the highest frequency shallow water normal mode found on a latitude-longitude grid (left), a hexagonal voronoi grid (centre), and a 'voronized' cubed sphere grid (right) (Weller et al. 2012).

computational-mode-like behaviour as parameters are varied. The important thing is to be aware of the ways in which linear wave propagation can be misrepresented, and their possible consequences, and for model developers to analyse for such behaviour at an early stage of model design.

Acknowledgements

The author is grateful to Colin Cotter, Dan Holdaway, Tom Melvin, Daniel Le Roux, David Long, Todd Ringler, Bill Skamarock, Andrew Staniforth, Mark Taylor, and Hilary Weller for valuable discussions on the topic of computational modes, many of which took place during the Isaac Newton Institute programme on Multiscale Numerics for the Atmosphere and Ocean, Autumn 2012.

References

Arakawa, A., and V.R. Lamb, (1977). Computational design of the basic dynamical processes of the UCLA general circulation model. In: Chang, J. (ed.) "General Circulation Models of the Atmosphere", Methods in Computational Physics, vol 17, pp172–265. San Diego: Academic Press.

Arakawa, A., and S. Moorthi (1988). Baroclinic instability in vertically discrete systems. *J. Atmos. Sci.*, **45**, 1688–1707.

Asselin, R. (1972). Frequency filter for time integrations. *Mon. Wea. Rev.*, **100**, 487–490.

Danilov, S. (2010). On the utility of triangular C-grid type discretization for numerical modeling of large-scale ocean flows. *Ocean Dyn.*, **60**, 1361–1369.

Durran, D.R. (2010). *Numerical Methods for Fluid Dynamics with Applications to Geophysics*. New York, Dordrecht, Heidelberg, London: Springer

Hollingsworth, A. (1995). A spurious mode in the 'Lorenz' arrangement of Φ and T which does not exist in the 'Charney Phillips' arrangement. ECMWF Technical Memorandum **211**.

Le Roux, D.Y. (2012). Spurious inertial oscillations in shallow-water models. *J. Comput. Phys.*, **231**, 7959–7987.

Le Roux, D.Y., V. Rostand, and B. Pouliot (2007). Analysis of numerically induced oscillations in 2D finite-element shallow-water models. Part I: Inertia-gravity waves. *SIAM J. Sci. Comp.*, **29**, 331–360.

Le Roux, D.Y, A. Sène, V. Rostand, E. Hanert (2005). On some spurious mode issues in shallow-water models using a linear algebra approach. *Ocean Modelling*, **10**, 83–94.

Long, D.J., and J. Thuburn (2011). Numerical wave propagation on non-uniform one-dimensional staggered grids. *J. Comput. Phys.*, **230**, 2643–2659.

Ničković, S., M.B. Gavrilov, and I.A. Tosić (2002). Geostrophic adjustment on hexagonal grids. *Mon. Wea. Rev.*, **130**, 668–683.

Randall, D.A. (1994). Geostrophic adjustment and the finite-difference shallow-water equations. *Mon. Wea. Rev.*, **122**, 1371–1377.

Robert, A.J. (1966). The integration of a low order spectral form of the primitive meteorological equations. *J. Meteor. Soc. Japan*, **44**, 237–245.

Rostand, V., D.Y. Le Roux, and G. Carey (2008). Kernel analysis of the discretized finite difference and finite element shallow-water models. *SIAM J. Sci. Comp.*, **31**, 531–556.

Schneider, E.K. (1987). An inconsistency in vertical discretization in some atmospheric models. *Mon. Wea. Rev.*, **115**, 2166–2169.

Staniforth, A., and J. Thuburn (2012). Horizontal grids for global weather and climate prediction models: A review. *Quart. J. Roy. Meteorol. Soc.*, **138**, 1–26.

Thuburn, J. (2006). Vertical discretizations giving optimal representation of normal modes: Sensitivity to the form of the pressure gradient term. *Quart. J. Roy. Meteorol. Soc.*, **132**, 2809–2825.

Thuburn, J. (2008). Numerical wave propagation on the hexagonal C-grid. *J. Comput. Phys.*, **227**, 5836–5858.

Thuburn, J. and T.J. Woollings (2005). Vertical discretizations for compressible Euler equation atmospheric models giving optimal representation of normal modes. *J. Comput. Phys.*, **203**, 386–404.

Tokioka, T. (1978). Some considerations on vertical differencing. *J. Meteorol. Soc. Japan*, **56**, 98–111.

Toy, M.D. and D.A. Randall (2007). Comment on the article "Vertical discretizations for compressible Euler equation atmospheric models giving optimal representation of normal mode" by Thuburn and Woollings. *J. Comput. Phys.*, **223**, 82–88.

Trefethen L.N. (1982). Group velocity in finite difference schemes. *SIAM Rev.*, **23**, 113–136.

Vichnevetsky R. (1987). Wave propagation and reflection in irregular grids for hyperbolic equations. *Appl. Numer. Math.*, **3**, 133–166.

Walters R.A., and G.F. Carey, (1984). Numerical noise in ocean and esturine models. *Adv. Water Resour.*, **7**, 15–20.

Weller, H., J. Thuburn, and C.J. Cotter (2012). Computational Modes and Grid Imprinting on Five Quasi-Uniform Spherical C-Grids. *Mon. Weather Rev.*, **140**, 2734–2755.

Williams, P.D. (2009). A proposed modification to the Robert-Asselin time filter. *Mon. Wea. Rev.*, **137**, 253–2546.